Mechanics of Composite Materials, Vol. 50, No. 3, July, 2014 (Russian Original Vol. 50, No. 3, May-June, 2014)

THEORETICAL-EXPERIMENTAL METHOD FOR DETERMINING THE PARAMETERS OF DAMPING BASED ON THE STUDY OF DAMPED FLEXURAL VIBRATIONS OF TEST SPECIMENS

2. AERODYNAMIC COMPONENT OF DAMPING

A. G. Egorov,[1*] A. M. Kamalutdinov,[1] A. N. Nuriev,[1] and V. N. Paimushin[2]

Keywords: *damping, flexural vibrations of plates, flow around a vibrating plate, computational fluid dynamics, direct numerical simulation, drag coefficient*

The aerodynamic component of damping of a vibrating plate in the range of parameters characteristic of damped flexural vibrations of test specimens is investigated. On the basis of a large series of numerical simulations in the dynamics of two-dimensional flow of gas around a plate, we managed to suggest a unified approximating equation for the damping constant in terms of dimensionless parameters of the process considered.

Introduction

Investigations into the forced and free mechanical vibrations of plates in a stationary viscous fluid (gas) have recently been of increased interest. One of their practical applications is connected with measurements of the damping properties of materials [1]. In addition, the results of these investigations can be employed in such areas as atomic force microscopy [2-5], sensors and drives of heads on micromechanical generators [6-9], cooling devices [10, 11], robotics [12-14], the stability of oil platforms [15], and damping the vibrations of liquids in fuel tanks [16, 17].

One of the primary goals in this class of problems is prediction of the forces acting on a vibrating plate on the fluid (gas) side. It is assumed that the aerodynamic interaction can be reduced to the inertial effect of an apparent mass and to the aerodynamic damping (see, for example, [18-20]). The inertial effect decreases the frequency, while the aerodynamic damping increases the decrement of vibrations of the plate compared with it in vacuum.

[1]Kazan (Volga region) Federal University, Lobachevskii Institute of Mathematics and Mechanics, Kazan, Russia
[2]Kazan National Research Technological University, Institute of Aviation, Land Transport, and Energy, Kazan, Russia
[*]Corresponding author; e-mail: aegorov0@gmail.com

Translated from Mekhanika Kompozitnykh Materialov, Vol. 50, No. 3, pp. 379-396 , May-June, 2014. Original article submitted October 11, 2013.

In the general case, the problem on account of aerodynamic forces acting on a cantilever plate is extremely complicated, mainly because of the complexity of three-dimensional gas flows caused by vibration of the plate. The known approaches [2, 18] to its solution are based on the assumption that the length L of the plate considerably exceeds its width b and thickness h. In this case, at low structural vibration modes, the length of the vibrational wave is much greater than deviations of the plate, as a result of which it can be regarded as locally planar. In this case, the three-dimensional phenomena relating to gas flows along the plate length, including the separation of vortices from its butt end, are neglected, and the aerodynamic forces in each cross section of the beam are determined by examining the plane motion of gas caused by harmonic vibrations of a thin rigid plate. Such a plate, having a rectangular cross section, serves as a mobile boundary for the surrounding medium.

However, even in the plane approximation, the problem of determination of the aerodynamic forces acting on a harmonically vibrating plate has not yet been solved in full. From a dimensional analysis it is known that, along with the geometrical parameter $\Delta = h/b$, the forces have to depend on two more dimensionless quantities, for which (see, for example, [21, 22]) the ratio $\kappa = a/b$ of vibration amplitude to width of the plate and the Stokes parameter β, playing the role of the vibrational Reynolds number, are usually assumed. In many studies, κ is replaced by its analogue, the Keulegan–Carpenter number $\mathrm{KC} = 2\pi\kappa$. Theoretically substantiated results are available only for vibrations with an infinitesimal amplitude ($\kappa \to 0$). They date back to the original study by Stokes [23], who considered vibrations of an infinite cylinder in a viscous fluid. A similar analysis for a plate was carried out in [24, 25]. In these studies, the flow of fluid was described by linearized Navier–Stokes equations, with inertial terms being neglected. Therefore, the force per length unit of a body, described in terms of the drag coefficient, depends only on the Stokes parameter β.

In many experimental [16, 26, 27], theoretical [17, 28, 29], and computational [11, 15, 20] studies, another limiting case was examined, namely great-amplitude vibrations, when the viscous dissipation of energy can be neglected compared with the energy of the vortices formed during the period of vibration on the lateral faces of the plate. In this case, the Stokes parameter is excluded from the number of determining parameters, and the drag coefficient depends solely on the dimensionless vibration amplitude κ.

The intermediate range of variations in the dimensionless vibration amplitude κ, where the viscous and inertial effects are commensurable, is investigated much more poorly. The experimental and numerical results available either cover a small part of the range examined or are distant from the region of values of the parameters realized in a laboratory to determine the damping properties of materials by investigating the free flexural vibrations of test specimens [1].

The dimensionless vibration amplitudes $\kappa < 2$ realized in laboratory investigations lie mostly in the intermediate range; the parameter β takes values from several tens to several hundreds, while the dimensionless thickness Δ of the plate — from several tenths to several hundredths. In this case, the Reynolds number $\mathrm{Re} = 2\pi\beta\kappa$ does not exceed several thousands, and thus, a direct numerical simulation of plane aerodynamic fields around a vibrating plate does not require an excessively detailed discretization. The use of moderate meshes, with about several hundred thousand nodes, allows one to perform a great (more than 200) series of computational experiments on the dynamics of a two-dimensional flow of gas around a plate and to calculate the complex drag coefficient over the entire region of the parameters κ, β, and Δ we are interested in.

1. Statement of the Problem

Let us consider an elastic plate of length L, width b, and thickness h ($h << b << L$) (Fig. 1). One of its ends is rigidly fixed, but the second is free. As soon as the plate is disturbed from the equilibrium, it starts to vibrate harmonically in the surrounding air. As experiments show, the frequency of these vibrations ω weakly varies in the vicinity of the basic eigenfrequency ω_0 of flexural vibrations of the plate, while the amplitude A weakly decays with time t because of air resistance and internal damping. The problem consists in determining the laws of slow variations in the amplitude and frequency. We will characterize the respective quantities by using the logarithmic decrement of vibrations $\delta(A)$ and the relative variation in frequency $\Omega(A)$ as functions of the current amplitude A of flexural vibrations of the plate:

$$\delta = -\frac{2\pi}{A\omega_0}\frac{dA}{dt}, \quad \Omega = \frac{\omega_0 - \omega}{\omega_0}.$$

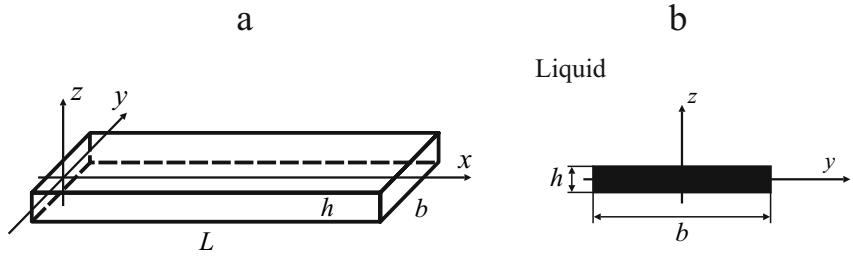

Fig. 1. Schematic of a plate for the problem on its vibration (a) and the schematic of a 2-dimensional hydrodynamic problem (b).

The equation describing vibrations of a plate according to a cylindrical flexural mode has the form

$$\frac{Ebh^3}{12} w^{\mathrm{IV}} + \rho bh\ddot{w} = H + P. \tag{1}$$

Hereinafter, the primes designate differentiation with respect to x and dots — with respect to time t; w is the displacement of middle line of the plate along the z axis; H and P are the forces of internal friction and aerodynamic resistance; ρ and E are the effective density and Young's modulus of plate material. The boundary conditions correspond to a rigid fixation at $x = 0$ and to a free end at $x = L$.

The drag forces are smaller than the elastic one. Therefore, to a first approximation, we may assume that $H = P = 0$. In this case, as is known, the basic vibration mode takes the form

$$w = A\cos(\omega_0 t)\ W(x/L). \tag{2}$$

The constants A and ω_0 represent the amplitude and eigenfrequency of the basic mode, and the profile W of vibrations [$W(1) = 1$] is described by the formula

$$W(x) = \frac{1}{2}(\cosh kx - \cos kx) - \frac{1}{2}\cdot\frac{\cosh k + \cos k}{\sinh k + \sin k}(\sinh kx - \sin kx).$$

The value of $k = 1.8751$ is the smallest positive root of the equation $\cos k \cdot \cosh k = -1$, and the frequency of natural vibrations is

$$\omega_0 = k^2 \frac{h}{L^2}\sqrt{\frac{E}{12\rho}}.$$

Owing to the presence of small ($\sim \varepsilon$) forces in the right-hand side of Eq. (1), the vibration amplitude A and frequency ω_0 in Eq. (2) do not remain constant, but slowly vary in time. An analysis of such a variation can be carried out by introducing, along with the fast time t, a slow time $\tau = \varepsilon t$ and performing a two-scale asymptotic expansion. Omitting details of this procedure, we present the final result:

$$\delta = 2\pi F_0^{-1}\frac{\{\sin\omega_0 t\langle(P+H)W\rangle\}}{\langle W^2\rangle},\quad \Omega = F_0^{-1}\frac{\{\cos\omega_0 t\langle(P+H)W\rangle\}}{\langle W^2\rangle},\quad F_0 = \rho bhA\omega_0^2. \tag{3}$$

Hereinafter, the angular brackets designate averaging over the spatial coordinate x, while the braces mean time averaging.

In using Eqs. (3), assuming the flexurale vibrations of form (2) with a constant value of A, it is necessary

(1) to calculate the force of internal friction $H(t, x; A)$,

(2) to solve the aerodynamic problem and calculate the drag force $P(t, x; A)$, and

(3) having calculated the averages in Eqs. (3), to determine the required dependences $\delta(A)$ and $\Omega(A)$.

It is obvious that, in view of linearity of the right-hand sides parts of Eqs. (3), the different components of drag forces can be calculated independently from each other. Leaving aside the question on the contribution of internal friction to the damping forces, we will pass to determination of the aerodynamic component.

2. Aerodynamic Problem

The force $P(x,t)$ per unit length of the plate in Eq. (1) describes the action exerted on the plate by the environment, which is regarded as an incompressible Newtonian fluid. The density and kinematic viscosity of the fluid is designated by ρ_0 and ν, respectively. We take into account the fact that the length of the plate is much greater than the other two its characteristic dimensions, while the length of the vibration wave of the basic structural mode considerably exceeds its displacements. Therefore, the plate can be considered locally planar. The aerodynamic force $P(x,t)$ is found during solving the plane problem on fluid flow caused by vibrations of an infinitely extended thin rigid plate (Fig. 1b). Such a plate plays the role of a mobile solid boundary for the air surrounding it. In each given cross section x, the law of motion of this boundary is given as $z = a(x)\cos\omega_0 t,\ a = AW(x/L)$.

Let us pass to a moving system of coordinates rigidly connected to the plate and introduce, in a standard way, a fictitious pressure p [25] equal to the sum of the true pressure and the inertial component $\rho_0 az\omega_0^2\cos\omega_0 t$. Normalizing the spatial coordinates to b, the time to ω_0^{-1}, the flow rate $\boldsymbol{v} = (v_y, v_z)$ of fluid to $a\omega_0$, the fictitious pressure to $\rho_0 a^2\omega_0^2$, and retaining the previous designations of dimensionless variables, we present the Navier–Stokes equations in the form

$$\nabla\cdot\boldsymbol{v} = 0,\quad \frac{\partial\boldsymbol{v}}{\partial t} + \kappa\boldsymbol{v}\cdot\nabla\boldsymbol{v} = -\kappa\nabla p + \frac{1}{2\pi\beta}\Delta\boldsymbol{v}. \tag{4}$$

The dimensionless quantities

$$\beta = \frac{b^2\omega_0}{2\pi\nu},\quad \kappa = \frac{a}{b}$$

determine the Stokes parameter and (accurate to the factor 2π) the Keulegan–Carpenter parameter, respectively. The dimensionless frequency of vibrations β is the squared ratio of plate width to the thickness of the nonstationary boundary layer, and the dimensionless amplitude of vibrations κ is the ratio between the vibration amplitude and width of the plate. One more dimensionless parameter of the problem, $\Delta = h/b$, specifies the shape of the plate.

Equations (4) are supplemented with the boundary conditions of adhesion on the boundary Γ of the plate

$$\Gamma = \Gamma_y^+ + \Gamma_y^- + \Gamma_z^+ + \Gamma_z^-,\quad \Gamma_y^\pm = \left\{y = \pm\frac{1}{2}, |z| < \frac{\Delta}{2}\right\},\quad \Gamma_z^\pm = \left\{z = \pm\frac{\Delta}{2}, |y| < \frac{1}{2}\right\}$$

and with the flow rate of fluid assigned at infinity

$$\boldsymbol{v}\big|_\Gamma = 0,\quad v_y(\infty) = 0,\quad v_z(\infty) = \sin t. \tag{5}$$

After solving the problem (4), (5), the aerodynamic force P acting on the plate is calculated as

$$P = \rho_0 ab^2\omega_0^2\left[\Delta\cos t + \kappa\left(\int\limits_{\Gamma_z^-} p\,d\gamma - \int\limits_{\Gamma_z^+} p\,d\gamma\right) + \frac{1}{2\pi\beta}\left(\int\limits_{\Gamma_y^-}\frac{\partial v_z}{\partial y}\,d\gamma - \int\limits_{\Gamma_y^+}\frac{\partial v_z}{\partial y}\,d\gamma\right)\right].$$

The first term is the Krylov–Froude force and the other two determine the normal and shear components of the aerodynamic force.

We should note that the problem (4), (5) also describes the flow of an oscillating fluid around a motionless plate. However, the pressure p in Eqs. (4) then has to be treated as the true and not fictitious pressure. Consequently, the aerodynamic force acting on a motionless plate in an oscillating flow minus the Krylov–Froude force will coincide with the force acting on the vibrating plate on the part of gas motionless at infinity. Therefore, in our situation, the numerous theoretical and

experimental results on determination of the drag force of a motionless plate to an oscillating flow can be used. In such a case, the forces acting on a body are usually investigated by using the Morrison approximation [20, 26], according to which

$$P = -\frac{\pi}{4}\rho_0 b^2 C_M \frac{du}{dt} - \frac{1}{2}\rho_0 b C_D |u| u.$$

Here, $u = -AW(x/L)\omega_0 \sin\omega_0 t$ is the flow rate at infinity, C_M is the factor of apparent masses, and C_D is the drag coefficient. The factors C_M and C_D are functions of the dimensionless parameters $\kappa, \beta, \text{and}\, \Delta$ of the problem, which, accurate to constant multipliers, coincide with values of the basic harmonics $\{P\cos\omega_0 t\}$ and $\{P\sin\omega_0 t\}$ of the hydrodynamic force [26]. In terms of these factors, formulas (3), determining the vibration decrement and the variation in vibration frequency of the plate, can be written in the form

$$\delta = \frac{4}{3}\frac{\rho_0}{\rho}\frac{A}{h}\frac{\langle C_D W^3\rangle}{\langle W^2\rangle}, \quad \Omega = \frac{\pi}{8}\frac{\rho_0}{\rho}\frac{b}{h}\frac{\langle (C_M + C_M^{KF})W^2\rangle}{\langle W^2\rangle}. \tag{6}$$

The presence of the additional term $C_M^{KF} = 4\pi^{-1}\Delta$ is associated with existence of the Krylov–Froude forces.

Thus, to determine the decrement δ and the relative frequency Ω of vibrations of the plate, we have first to calculate the hydrodynamic factors C_D and C_M as functions of the dimensionless parameters s $\kappa, \beta, \text{and}\, \Delta$. In the case considered, the dimensionless frequency β varies from several tens to hundreds, the dimensionless thickness of the plate Δ — from several tenths to several hundredths, and the dimensionless vibration amplitude k lies in the range [0, 3].

3. Small and Large Vibration Amplitudes

Rigorous theoretical results for the hydrodynamic factors C_D and C_M are known only in the limiting case $\kappa \to 0$ of small-amplitude vibrations (the so-called Stokes approximation). At $\Delta < 0.3$, we have [18, 25]

$$\kappa \to 0: \quad C_D = \frac{4.61}{\kappa\sqrt{\beta}}, \quad C_M = 1.$$

Calculations according to Eqs. (6) give

$$\kappa \to 0: \quad \delta = \frac{6.14}{\sqrt{\beta}}\cdot\frac{\rho_0}{\rho}\cdot\frac{b}{h} = 6.14\frac{\rho_0}{\rho h}\sqrt{\frac{2\pi\nu}{\omega_0}}, \quad \Omega = \frac{\pi}{8}\cdot\frac{\rho_0}{\rho}\cdot\frac{b}{h} + \frac{\rho_0}{2\rho}. \tag{7}$$

With growing dimensionless vibration amplitude, the flow pattern is determined by the separation of intense vortices from ends of the plate. The viscous effects play an auxiliary role (because it is only the geometry that determines the place of separation of the vortices). Accordingly, the only parameter considering the viscosity, β, ceases to be determining, and the hydrodynamic factors become functions of κ and Δ. To find these dependences, we will consider the classical Keulegan–Carpenter experiments [26]. According to these experiments, performed for small values of Δ, the drag coefficient in the range $\kappa > 1$ can be approximated by the formula

$$\kappa > 1: \quad C_D = \frac{6.2}{\sqrt{\kappa}}.$$

For the vibration decrement, we have from Eqs. (6)

$$\kappa > 1: \quad \delta = 7\frac{\rho_0}{\rho}\frac{\sqrt{Ab}}{h}. \tag{8}$$

According to [26], with increasing κ, the factor of apparent masses first grows, reaching its maximum value equal to about 2 at $\kappa \approx 1$, and then decreases. Assuming that $C_M < 2$ and estimating the quantity Ω according to Eqs. (6), we find that, for typical values of parameters, the relative variation Ω in frequency does not exceed 0.001. Such small changes in

frequency cannot be measured on our experimental setup [1]. Therefore, we can presume that the aerodynamic interaction cannot change the vibration frequency of a plate.

The situation is quite different for the vibration decrement. Assuming for C_D the Keulegan–Carpenter approximation and estimating the vibration decrement according to Eqs. (6), we find that, at typical values of parameters, the decrement δ is a quantity of the order of hundredths. Exactly the values of δ of such an order were observed and registered with confidence in experiments [1] on the damping of flexural vibrations of test specimens.

It is interesting that, in the limit of small amplitudes [see Eqs. (7)], the aerodynamic component of vibration decrement no longer depends on the width of the plate, while at large amplitudes [see Eqs. (8)], it ceases to depend on the length of the plate and the elastic properties determining the vibration eigenfrequency ω_0.

4. Intermediate Vibration Amplitudes

The drag coefficient depends on all the three dimensionless parameters s $\kappa, \beta, \text{and}\, \Delta$ in a complex way. To determine the quantities C_M and C_D as functions of the parameters, it is necessary to carry out a direct numerical simulation (DNS) of flow around a two-dimensional vibrating plate by using solutions to the Navier–Stokes equations. The corresponding numerical calculations were performed in the OpenFOAM (Open Field Operation and Manipulation) package of computational hydrodynamics (CFD), based on a finite-volume approach to the solution of equations of hydrodynamics.

In the calculations, we considered a rectangular $30b \times 30b$ region with a plate located at its center. On the input and output boundaries of the region, we assigned a zero tangential speed and problem-adapted conditions implying the assignment of pressure on a half-period of the inflow of fluid through the boundary and of a pressure gradient on a half-period of outflow. Slippage conditions were set on the lateral boundaries of the region, and adhesion conditions were assumed on the plate.

To discretize the calculation domain, orthogonal block meshes created by using the blockMesh utility entering into the OpenFOAM package were employed. The resolution of the meshes near the plate was increased by condensing them in the horizontal and vertical directions. The numbers of cells neighboring with the end and the lateral face of the plate were 20 and 80, respectively. The degree of condensation of the mesh varied in the range of 40-50 along the y axis and of 15-20 along the z axis. The number of nodes in the meshes did not exceed $3 \cdot 10^5$. In discretization, a combined arrangement of nodes was employed; the discrete values of speed and pressure were localized at the centers of calculation cells of the mesh. The volume integrals were calculated by using the general Gauss procedure, according to which transition from volume to surface integrals is carried out. Further, the surface integrals were presented as the sum of integrals over faces of the cell and calculated approximately by the formula of average rectangles. Values of the function and the normal derivatives on the cell surface for internal cells of the calculation domain were interpolated from those at the centers of neighboring cells. The pressure gradient was interpolated linearly. To interpolate variables in the convective terms, the nonlinear NVD "Gamma" scheme suggested in [31] was employed. The normal gradients of speed on surfaces of the cell, necessary for discretization of the Laplace operator, were calculated from the speed at the centers of neighboring cells according to the symmetric second-order scheme.

The time discretization of the system was carried out according to the implicit Euler scheme. The time step in all calculations was chosen such that the maximum Courant number did not exceed 0.1.

The solution of the discrete problem in the package is based on the "segregated approach" of a separate solution of speed and pressure equations. The problem was solved by using the icoFoam program realizing the PISO (Pressure Implicit Splitt Operator) algorithm [32-34]. The basic parameter of this algorithm — the number of corrections — for the meshes used here was equal to three. To solve the system of equations for pressure, the preconditioned conjugate gradient (PCG) method with a geometric-algebraic multigrid (GAMG) preconditioner was employed. In realizing the GAMG, for smoothing, we used the Gauss–Seidel method with one and two pre- and postrelaxations, respectively, and for agglomeration of mesh cells — the faceAreaPair algorithm [35]. The system of equations for speeds was solved by the method of biconjugate gradients (PBiCG) with a preconditioner based on an incomplete LU factorization. At all stages, the convergence was carried out up to the values of residual smaller than 10^{-8}. In more detail, the numerical scheme is described in [36].

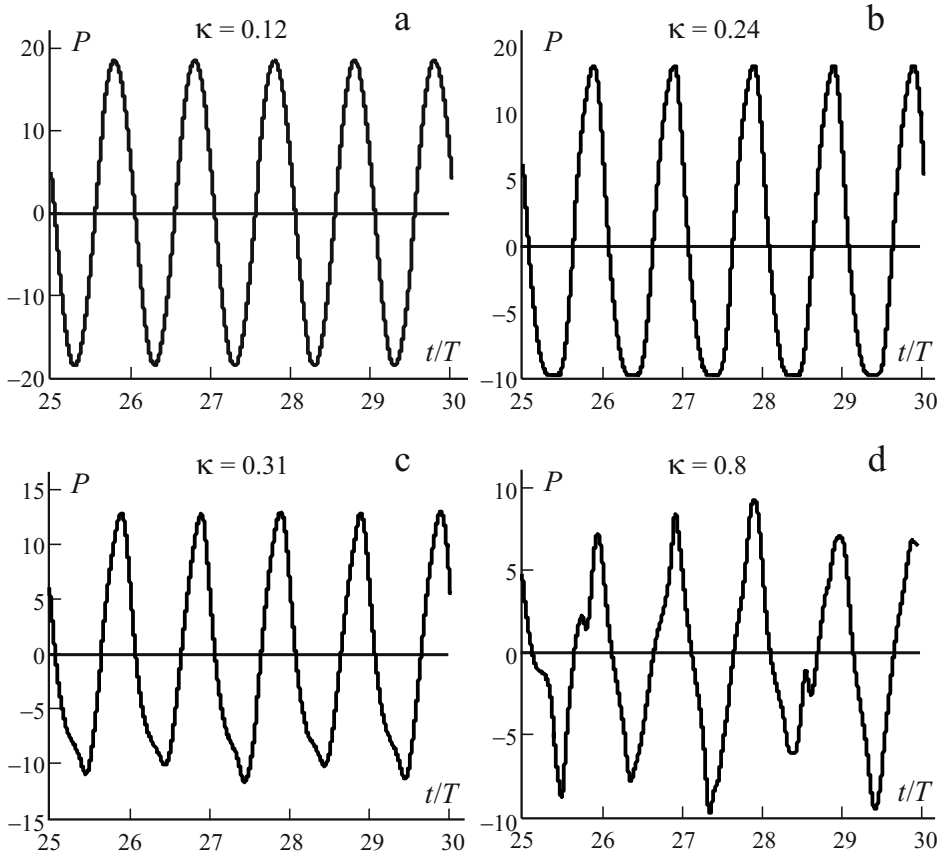

Fig. 2. Resistance force P vs time t/T at $\Delta = 1/10$ and $\beta = 103$.

All calculations were distributed according to the MPI technology and performed by using the method of decomposition of the calculation region. For this purpose, the region was divided into several vertical subregions. The subproblems in each subregion were calculated on different cores of processor.

The calculations were carried out for plates of dimensionless thicknesses $\Delta = 0.05$, 0.1, 0.22, and 0.32 at the dimensionless vibration frequencies $\beta = 58.33$, 103, 200, and 1000. The above-mentioned parameters cover the entire range of parameters used in experiments [1]. For each fixed β and Δ, a series of calculations (15-20) were carried out at different values of the dimensionless vibration amplitude κ. The upper bound of κ was determined by the condition $\mathrm{Re} = 2\pi\kappa\beta < 4000$; this allowed us to use moderate meshes with 10^5 nodes. In total, 200 such calculations were performed. Each of them consisted in determination of the aerodynamic fields and the forces acting on the plate during 40 periods of vibrations. In all cases, the initial conditions corresponded to the condition of rest. Leaving aside a detailed aerodynamic analysis of flow patterns, let us pass to calculation of the drag coefficient $C_D(\kappa, \beta, \Delta)$ and the vibration decrement δ according to Eqs. (6). In dimensionless variables,

$$C_D(\kappa, \beta, \Delta) = \frac{1}{t_{\max} - t_{\min}} \int_{t_{\min}}^{t_{\max}} P(t; \kappa, \beta, \Delta) \sin t dt.$$

The averaging was carried out for all, except for the first, periods of vibrations: $t_{\min} = T$ and $t_{\max} = 40T$. Figure 2 illustrates a typical behavior of the relations $P(t)$ with growing dimensionless vibration amplitude of the plate. As seen, at small values of κ, the aerodynamic response $P(t)$ is a harmonic function (see Fig. 2a). Further (see Fig. 2b), the response is still periodic, but vibrations distinct from the basic vibration harmonic increase in it. They are mainly the third-order harmonics. With further growth in the parameter κ, the function $P(t)$ loses its strict periodicity (see Fig. 2c) and finally (see Fig. 2d) exhibits a chaotic behavior.

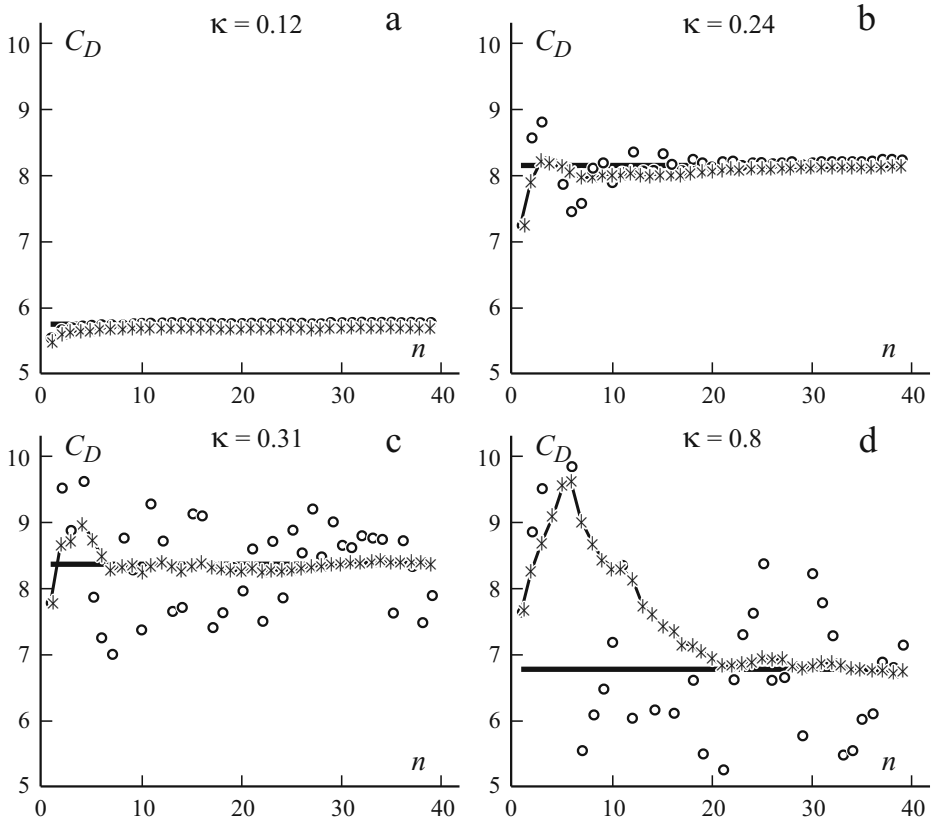

Fig. 3. Drag coefficients C_D (——), C_D^{glob} (–∗–), and C_D^{loc} (○) vs vibration period n at $\Delta = 1/10$ and $\beta = 103$.

The behavior of $P(t)$ mentioned directly affects the drag coefficient, as illustrated in Fig. 3. Along with the mean drag coefficient C_D, this figure also shows the local $C_D^{\text{loc}}(n)$ and "accumulated" $C_D^{\text{glob}}(n)$ drag coefficients

$$C_D^{\text{loc}}(n) = \frac{1}{T}\int_{nT}^{(n+1)T} P_D(t)\sin t dt, \quad C_D^{\text{glob}}(n) = \frac{1}{nT}\int_{T}^{(n+1)T} P_D(t)\sin t dt.$$

As seen, at small κ, the transition to a periodic mode occurs on the second or third period of vibrations (see Fig. 3a), but with growing κ, this transition is delayed (see Fig. 3b). Further, aperiodic (see Fig. 3c) and chaotic (see Fig. 3d) flow modes are realized. But even in the latter case, as shown by the behavior of the "accumulated" drag coefficient, averaging over 40 periods of vibrations, used in our calculations, proves to be sufficient for determining the average drag coefficient with an admissible accuracy.

The dependences $C_D(\kappa)$ calculated at $\Delta = 0.1$ and different values of β are shown in Fig. 4a, and those at fixed β and different values of Δ — in Fig. 4b.

As can be seen, the $C_D(\kappa)$ curves have a characteristic *S* shape. At small κ, they approach the Stokes asymptotics, while at great κ — the Keulegan–Carpenter experimental relationship. The greater the parameter β and smaller the quantity Δ, the earlier (at smaller κ) the deviation from the Stokes asymptotics occurs and the earlier the Keulegan–Carpenter experimental curve is reached. In general, at fixed $\kappa > 0{,}1$, the drag coefficient C_D grows with increasing dimensionless vibration frequency and decreasing dimensionless thickness of the plate.

The reliability of calculation results is confirmed by the fact that the calculated $C_D(\kappa)$ curves, at all values of the parameters β and Δ, approach the theoretically substantiated asymptotics at small κ and the known experimental dependence at great κ. An additional argument is the quite satisfactory agreement between the calculated and experimental data [26]

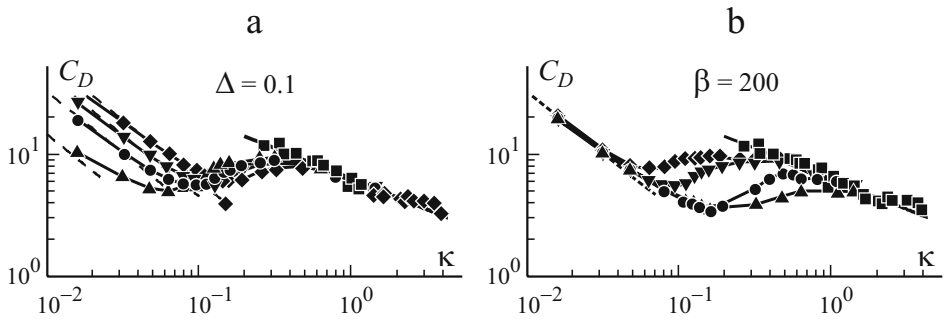

Fig. 4. Drag coefficient C_D vs κ [$\beta = 58.33$ (♦), 103 (▼), 200 (●), and 1000 (▲) (a) and $\Delta = 0.05$ (♦), 0.1 (▼), 0.022 (●), and 0.32 (▲) (b)]. ■ — Keulegan–Carpenter experimental data and (——) — Stokes asymptotics.

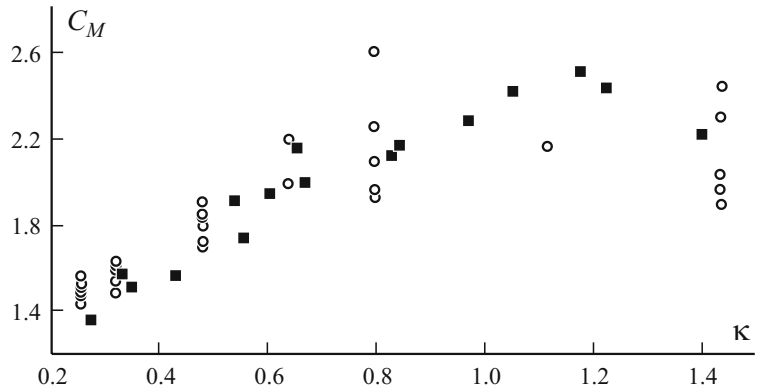

Fig. 5. Factor of apparent masses C_M as a function of κ at different values of the parameters β and Δ: ○ — calculation and ■ — experiment.

regarding the relation between the factor of apparent masses C_M and the dimensionless vibration amplitude κ (Fig. 5) on the entire calculation range of parameters.

5. Analytical Approximation of Results

Following [22], for an analytical approximation of numerical results, let us present the quantity C_D as the sum of two — viscous and vortical — components. For the first of them, we take the Stokes dependence, while the second is assigned according to the Keulegan–Carpenter experiments with a correction factor K:

$$C_D = C_D^{\text{vis}} + C_D^{\text{vort}}; \quad C_D^{\text{vis}} = \frac{4.61}{\kappa\sqrt{\beta}}, \quad C_D^{\text{vort}} = \frac{6.2}{\sqrt{\kappa}} K(\beta, \Delta, \kappa). \tag{9}$$

It is obvious that the correction factor K behaves similarly at all values of β and Δ, monotonically increasing with growth in κ from zero at $\kappa = 0$ to unity at $\kappa = \infty$. Moreover, as the analysis of numerical results shows, the $K(\kappa)$ graphs are practically identical at any values of β and Δ if the abscissa axis is extended in an appropriate way (depending on β and Δ):

$$K(\kappa, \Delta, \beta) = K(\xi), \quad \xi = \kappa\left[2 + 1.78\ln\Delta - \left[0.54 + 0.88\ln\Delta\right]\ln\beta\right]. \tag{10}$$

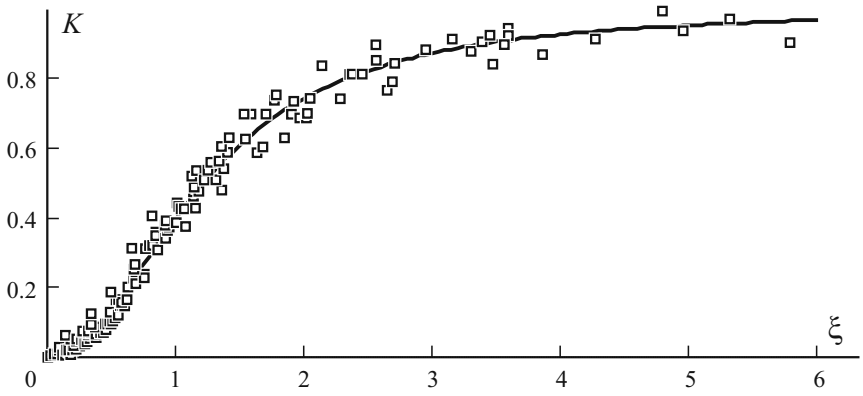

Fig. 6. Correction factor K as a function of the parameter ξ at different values of β and Δ: (□) — calculation and (——) — approximation.

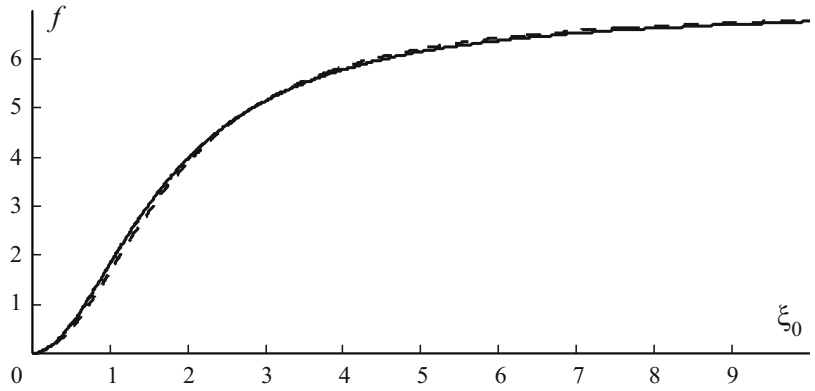

Fig. 7. Value of f as a function of the parameter ξ_0: (——) — calculation and (– – –) — approximation.

This fact is illustrated by the data shown in Fig. 6, where the dots denote the correction factor

$$K = \frac{\sqrt{\kappa}}{6.2}\left(C_D - C_D^{\text{vis}}\right)$$

in relation to the parameter ξ at different values of β and Δ.

As seen, the results of numerical experiment are grouped around one curve. This curve can be approximated with an admissible accuracy, for example, by using the simple dependence

$$K(\xi) = \frac{\xi^2}{\xi^2 + 1.7}. \tag{11}$$

Having determined the value of C_D by formulas (9)-(11), we calculate the vibration decrement δ from Eqs. (6). Designating by A/b the ratio of the current vibration amplitude of end of the plate to its width, we obtain

$$\begin{gathered}\delta = \frac{b\rho_0}{h\rho}F, \quad F = \frac{6.14}{\sqrt{\beta}} + \sqrt{\kappa_0}\, f(\xi_0), \\ \xi_0 = \kappa_0\left[2 + 1.78\ln\Delta - \left[0.54 + 0.88\ln\Delta\right]\ln\beta\right], \\ f\left(\xi_0\right) = 8.27\left\langle K\left(\xi_0 W(x)\right)W^{2.5}(x)\right\rangle \Big/ \left\langle u_0^2(x)\right\rangle.\end{gathered} \tag{12}$$

The determining vortical component of vibration decrement — the function f — is found from Eqs. (12) by simple integration (the solid line in Fig. 7). The asymptotic behavior of $f(\xi_0)$ at small and great values of ξ_0 is described by the formulas

$$\xi_0 \to \infty: \quad f(\xi_0) \approx 7.0, \quad \xi_0 \to 0: \quad f(\xi_0) \approx 2.73\xi_0^2.$$

Based on these asymptotics, we may suggest the following approximation formula for calculating $f(\xi_0)$:

$$f(\xi_0) = 7\frac{\xi_0^2}{\xi_0^2 + 3.2}. \tag{13}$$

As seen, this dependence well describes the behavior of $f(\xi_0)$ on the whole range of the parameter ξ_0.

Acknowledgments. This study was carried out within the framework of the Federal Targeted Program "Scientific and Scientific-Pedagogical Personnel of the Innovative Russia" for 2009-2013, created by order of the Russian Ministry of Education and Science of March, 22, 2012, No. 223 and July, 13, 2012, No. 1/22/3, on the subject "Development of a theoretical-experimental method to examine the damped vibrations with account of internal and aerodynamic external damping and to investigate the problems on propagation of sound waves through single-layer and sandwich panels in order to create calculation procedures for sound absorption parameters" (state contract No. 2012-1.2.1-12-000-1002-030)

REFERENCES

1. V. N. Paimushin, V. A. Firsov, I. Gyunal, and A. G. Egorov, "Theoretical-experimental method for determining the parameters of damping based on the study of damped flexural vibrations of test specimens. 1. Experimental basis," Mech. Compos. Mater., **50**, No. 2, 127-136 (2014).
2. J. E. Sader, "Frequency response of cantilever beams immersed in viscous fluids with applications to the atomic force microscope," J. Appl. Phys., **84**, No. 1, 64-76 (1998).
3. S. Kirstein, M. Mertesdorf, and M. Schoenhoff, "The influence of a viscous fluid on the vibration dynamics of scanning near-field optical microscopy fiber probes and atomic force microscopy cantilevers," J. Appl. Phys., **84**, No. 4, 1782-1790 (1998).
4. A. Maali, C. Hurth, R. Boisgard, C. Jai, T. Cohen-Bouhacina, and J.-P. Aimer, "Hydrodynamics of oscillating atomic force microscopy cantilevers in viscous fluids," J. Appl. Phys., **97**, No. 7, Art. 074907 (2005).
5. S. Basak, A. Raman, and S. V. Garimella, "Hydrodynamic loading of microcantilevers vibrating in viscous fluids," J. Appl. Phys., **99**, No. 11, Art. 114906 (2006).
6. H. Hosaka, K. Itao, and S. Kuroda, "Damping characteristics of beam-shaped micro-oscillators," Sensors and Actuators A: Physical, **49**, Nos. 1-2, 87-95 (1995).
7. M. Kimber, S. V. Garimella, and A. Raman, "Local heat transfer coefficients induced by piezoelectrically actuated vibrating cantilevers," Trans. ASME J. Heat Transf., **129**, No. 9, 1168-1176 (2007).
8. M. Kimber, R. Lonergan, and S. V. Garimella, "Experimental study of aerodynamic damping in arrays of vibrating cantilevers," J. Fluids Struct., **5**, No. 8, 1334-1347 (2009).
9. C. Castille, I. Dufour, and C. Lucat, "Longitudinal vibration mode of piezoelectric thick-film cantilever-based sensors in liquid media," Appl. Phys. Lett., **96**, Art. 154102 (2010).
10. M. Kimber and S. V. Garimella, "Measurement and prediction of the cooling characteristics of a generalized vibrating piezoelectric fan," Int. J. Heat Mass Transf., **52**, Nos. 19-20, 4470-4478 (2009).
11. R. A. Bidkar, M. Kimber, A. Raman, A. K. Bajaj, and S. V. Garimella, "Nonlinear aerodynamic damping of sharp-edged flexible beams oscillating at low Keulegan–Carpenter numbers," J. Fluid Mech., **634**, 269-289 (2009).
12. W. Shyy, M. Berg, and D. Ljungqvist, "Flapping and flexible wings for biological and micro air vehicles," Progr. Aerospace Sci., **35**, No. 5, 455-505 (1999).

13. Z. Chen, S. Shatara, and X. Tan, "Modeling of biomimetic robotic fish propelled by an ionic polymer-metal composite caudal fin," IEEE/ASME Trans. on Mechatronics, **13**, No. 5, 519-529 (2010).
14. M. Aureli, V. Kopman, and M. Porfiri, "Free-locomotion of underwater vehicles actuated by ionic polymer metal composites," IEEE/ASME Trans. on Mechatronics, **15**, No. 4, 603-614 (2010).
15. L. Tao and K. Thiagarajan, "Low KC flow regimes of oscillating sharp edges. I. Vortex shedding observation," Appl. Ocean Res., **25**, No. 2, 21-35 (2003).
16. G. N. Mikishev, "Experimental methods in the dynamics of space vehicles," Mashinostroenie, Moscow (1978).
17. V. A. Buzhinskii, Vibrations of Bodies with Sharp Edges in an Incompressible Low-Viscosity Fluid and Some Problems of the Hydrodynamics of Space Vehicles, PhD. Thesis, Korolev (2003).
18. M. Aureli, M. E. Basaran, and M. Porfiri, "Nonlinear finite amplitude vibrations of sharp-edged beams in viscous fluids," J. Sound Vibrat., **331**, 1624-1654 (2012).
19. M. Aureli and M. Porfiri, "Low frequency and large amplitude oscillations of cantilevers in viscous fluids," Appl. Phys. Lett., **96**, Art. 164102 (2010).
20. T. Sarpkaya, "Force on a circular cylinder in viscous oscillatory flow at low Keulegan–Carpenter numbers," J. Fluid Mech., **165**, 61-71 (1986).
21. G. Falcucci, M. Aureli, S. Ubertini, and M. Porfiri, "Transverse harmonic oscillations of laminae in viscous fluids: a lattice Boltzmann study," Philosoph. Trans. Roy. Soc. London. A: Math., Phys. and Eng. Sci., **369**, No. 1945, 2456-2466 (2011).
22. P. W. Bearman, M. J. Downie, J. M. R. Graham, and E. D. Obasaju, "Forces on cylinders in viscous oscillatory flow at low Keulegan–Carpenter numbers," J. Fluid Mechanics, **154**, 337-356 (1985).
23. G. G. Stokes, "On the effect of the internal friction of fluids on the motion of pendulums," Trans. Cambridge Philosoph. Soc., **9**, 8-106 (1851).
24. E. O. Tuck, "Calculation of unsteady flows due to unsteady motion of cylinders in a viscous fluid," J. Eng. Mathem., **3**, No. 1, 29-44 (1969).
25. D. R. Brumley, M. Willcox, and J. E. Sader, "Oscillation of cylinders of rectangular cross section immersed in fluid," Phys. Fluids, **22**, No. 5, Art. 052001 (2010).
26. G. H. Keulegan and L. H. Carpenter, "Forces on cylinders and plates in an oscillating fluid," J. Res. National Bureau Standards, **60**, No. 5, 423-440 (1958).
27. S. Singh, Forces on Bodies in Oscillatory Flow. PhD Thesis, University of London (1979).
28. J. M. R. Graham, "The forces on sharp-edged cylinders in oscillatory flow at low Keulegan–Carpenter numbers," J. Fluid Mech., **97**, No. 1, 331-346 (1980).
29. V. A. Buzhinskii, "Vortex damping of vibrations of a liquid in tanks with partitions," Prikl. Matem. Mekh., **62**, Iss. 2, 235-243 (1998).
30. M. A. Jones, "The separated flow of an inviscid fluid around a moving flat plate," J. Fluid Mechanics, **496**, 405-441 (2003).
31. H. Jasak, "Error analysis and estimation for the Finite Volume method with applications to fluid flows," PhD. Thesis, Imperial College, University of London (1996).
32. R. I. Issa, "Solution of implicitly discretised fluid flow equations by operator-splitting," J. Comput. Phys., **62**, 40-65 (1986).
33. J. H. Ferziger and M. Peric, Computational Methods for Fluid Dynamics, Springer, Berlin (2002).
34. H. K. Versteeg and W. Malalasekera, An Introduction to Computational Fluid Dynamics. The Finite Volume Method, Longman, New-York (1995).
35. E. O. Tuck, "Calculation of unsteady flows due to unsteady motion of cylinders in a viscous fluid," J. Eng. Mathem., **3**, No. 1, 29-44 (1969).
36. A. N. Nuriev and O. N. Zaytseva, "Solution to the problem on oscillating motion of a cylinder in a viscous liquid by using the OpenFOAM package," Vest. Kazan. Tekhnol. Univ., **8**, 116-123 (2013).